Advances in Applied Mathematics and Mechanics
Adv. Appl. Math. Mech., Vol. **8**, No. 4, pp. 536-555

DOI: 10.4208/aamm.2014.m844
August 2016

Differential Quadrature Analysis of Moving Load Problems

Xinwei Wang[1,*] and Chunhua Jin[1,2]

[1] *State Key Laboratory of Mechanics and Control of Mechanical Structures, Nanjing University of Aeronautics and Astronautics, Nanjing 210016, China*
[2] *School of Civil Engineering and Architecture, Nantong University, Nantong 224019, China*

Received 18 November 2014; Accepted (in revised version) 11 May 2015

Abstract. The differential quadrature method (DQM) has been successfully used in a variety of fields. Similar to the conventional point discrete methods such as the collocation method and finite difference method, however, the DQM has some difficulty in dealing with singular functions like the Dirac-delta function. In this paper, two modifications are introduced to overcome the difficulty encountered in solving differential equations with Dirac-delta functions by using the DQM. The moving point load is work-equivalent to loads applied at all grid points and the governing equation is numerically integrated before it is discretized in terms of the differential quadrature. With these modifications, static behavior and forced vibration of beams under a stationary or a moving point load are successfully analyzed by directly using the DQM. It is demonstrated that the modified DQM can yield very accurate solutions. The compactness and computational efficiency of the DQM are retained in solving the partial differential equations with a time dependent Dirac-delta function.

AMS subject classifications: 74S30, 65M99

Key words: Differential quadrature method, Dirac-delta function, moving point load, dynamic response, work-equivalent load.

1 Introduction

The differential quadrature method (DQM), originated by Bellman and his associates in the early 1970s [1,2], is a numerical technique for the solution of initial as well as boundary value problems. Since Bert and his coworkers first used the DQM to solve problems in structural mechanics in 1988 [3], the method has been well developed and applied successfully to a variety of initial and boundary value problems. Several efficient DQ

*Corresponding author.
Email: wangx@nuaa.edu.cn (X. W. Wang), jinch@ntu.edu.cn (C. H. Jin)

 ©2016 Global Science Press

https://doi.org/10.4208/aamm.2014.m844 Published online by Cambridge University Press

based time integration schemes are proposed by Fung [4,5], Shu et al. [6] and Chen and Tanaka [7]. The introduce of the special matrix product by Chen et al. [8] further simplifies the presentation of DQ equations and makes the DQM more efficient for solving non-linear problems. The DQM has been used in the fields of mathematics, physics and engineering. It is demonstrated that the DQM has the advantages of compactness and computational efficiency and can generate highly accurate numerical solutions. A vast body of literature exists. Relative research work in the area of structural mechanics and in general engineering has been well documented by Bert and Malik [9], Shu [10], Zong and Zhang [11] and Wang [12].

It is well known that the properties of the Dirac-delta function are not in the form of derivatives but in the form of integrals. Similar to the conventional point discrete methods such as the collocation method and finite difference method, the DQM has some difficulty in dealing with singular functions such as the Dirac-delta function. Numerical solutions may become oscillatory around the Dirac-delta function. To overcome this difficulty, the Dirac-delta function should be regularized to achieve a smoother representation and to stabilize the unwanted oscillatory behavior of solutions near the Dirac-delta function. A level-set finite difference approach for regularization of the Dirac-delta function is presented in [13].

From the literature review, it is rare to use the DQM directly for solutions of partial differential equation involving the Dirac-delta functions such as the problems of beams under a stationary or moving point load. For static analysis, the wavelet-based DQM [14] can yield reasonably accurate solutions by distributing the point load over a small region. Han et al. [15] also investigate the effect of different treatments of the concentrated load on the accuracy of DQ solutions. To obtain the equivalent load, linear, parabolic and cubic distributions are tried. They conclude that the solution accuracy is the highest if the point load is linearly distributed over a small region. The linear distribution is actually equivalent to the method used in [14] to deal with the concentrated load if the load is applied on a grid point. It is seen that the method to deal with the point load in [14,15] seems only physically sound but not mathematically clear. Over how small area should the load be uniformly or linearly distributed? Although the differential quadrature element method (DQEM) [16] can efficiently solve the static problem with a stationary point load, however, the DQEM is inconvenient for solving the moving loads problems which involve time dependent Dirac-delta functions, especially when several moving loads are involved.

To circumvent the difficulty encountered in dealing with the time-dependent Dirac-delta functions by using the DQM, the mixed Ritz-DQ method [17] and the mixed finite element-differential quadrature [18] are proposed. In these hybrid methods, Ritz method or finite element method is used to handle the time-dependent Dirac-delta functions and the DQM is merely used for the step by step time integration. Thus, directly using the DQM to solve the moving point load problem has not been reported thus far.

The objective of this paper is to propose a way to overcome the difficulty encountered in handling the time-dependent Dirac-delta function by using the DQM. Two modifica-

https://doi.org/10.4208/aamm.2014.m844 Published online by Cambridge University Press

tions are made. One is that the moving point load is work-equivalent to loads applied at all grid points and the other is that the governing equation is numerically integrated before it is discretized in terms of the differential quadrature. Detailed formulations are given. Beam structures under either a stationary or a moving point load are solved by using the modified DQM. Numerical results are compared to existing analytical and numerical solutions to verify the modified DQM. This paper ends with conclusions.

2 The modified DQM and formulations

2.1 Static analysis of a beam under a point load

Consider an Euler-Bernoulli beam of length L subjected to a concentrated load P at point x_p $(0\leq x_p\leq L)$, shown in Fig. 1. The governing equation is given by

$$EI\frac{d^4w}{dx^4}=P\delta(x-x_p) \tag{2.1}$$

or

$$EIw^{(4)}=P\delta(x-x_p), \tag{2.2}$$

where w is the deflection, EI is the bending rigidity and δ is the Dirac-delta function, respectively.

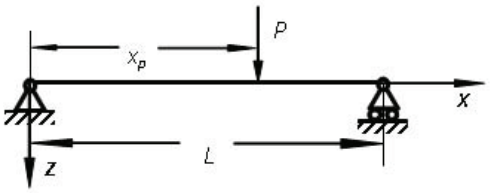


Figure 1: A simply supported beam under a concentrated load P.

It is well known that the Dirac-delta function has following properties,

$$\int_{-\infty}^{+\infty}\delta(x-x_p)dx=1 \tag{2.3}$$

and

$$\int_{-\infty}^{+\infty}P(x)\delta(x-x_p)dx=P(x_p). \tag{2.4}$$

To use the properties of the Dirac-delta function in the form of integrals, Eq. (2.2) is integrated as

$$\int_0^L EIw^{(4)}dx=\int_0^L P\delta(x-x_p)dx. \tag{2.5}$$

https://doi.org/10.4208/aamm.2014.m844 Published online by Cambridge University Press

Using Eq. (2.4), one has

$$\int_0^L P\delta(x-x_p)dx=P. \tag{2.6}$$

Thus

$$\int_0^L EIw^{(4)}dx=P. \tag{2.7}$$

To use the DQM, it is important that the left hand side of Eq. (2.5) or Eq. (2.7) is numerically integrated. There are many methods available for the numerical integration. For illustration, Gauss quadrature is used herein. Denote η_i $(i=2,3,\cdots,N-1)$ the $(N-2)$ Gauss points. Thus one has

$$\int_0^L EIw^{(4)}dx=\frac{L}{2}\int_{-1}^1 EIw^{(4)}d\eta=\frac{LEI}{2}\sum_{i=2}^{N-1}H_iw_i^{(4)}, \tag{2.8}$$

where H_i is the weight, $w_i^{(4)}=w^{(4)}(x_i)$, where $x_i=(1+\eta_i)L/2$, $(i=2,3,\cdots,N-1)$.

First assume that x_p is coincided with one of the integration points, i.e., $x_p=L(1+\eta_p)/2$. Since $\delta(x-x_p)=0$ for all points except point x_p, one has

$$EIw_i^{(4)}=0,\quad (i=2,3,\cdots,p-1,p+1,\cdots,N-1). \tag{2.9}$$

Therefore, Eq. (2.8) can be simplified as

$$\int_0^L EIw^{(4)}dx=\frac{LEIH_pw_p^{(4)}}{2}. \tag{2.10}$$

Combining Eqs. (2.6), (2.9) and (2.10) together yields

$$\begin{cases} EIw_p^{(4)}=\dfrac{2P}{LH_p}=F_p, \\ EIw_i^{(4)}=0,\quad (i=2,3,\cdots,p-1,p+1,\cdots,N-1). \end{cases} \tag{2.11}$$

The DQM is then used to approximate the fourth order derivatives at the $(N-2)$ inner grid points shown in Eq. (2.11). There are several grid distributions available in the literature [12]. For simplicity and reliability considerations, assume that the N grid points (ξ_i) used in the DQM are $\{-1,\ \eta_i(i=2,3,\cdots,N-1),\ +1\}$. In terms of the differential quadrature, Eq. (2.11) at all inner points can be written as

$$EI\sum_{j=1}^{N}D_{ij}w_j=F_i,\quad (i=2,3,\cdots,N-1), \tag{2.12}$$

https://doi.org/10.4208/aamm.2014.m844 Published online by Cambridge University Press

where D_{ij} is the weighting coefficient of the fourth order derivative with respect to x, w_j is the deflection at point $x_j=L(1+\xi_j)/2$, and F_i is given by

$$F_i=\begin{cases} 0, & i=2,3,\cdots,p-1,p+1,\cdots,N-1, \\ 2P/(LH_p), & i=p. \end{cases} \tag{2.13}$$

In general, the location of the applied load P is not coincided with any integration point. Thus a method called the work-equivalent method is proposed. The load P is first work-equivalent to a set of concentrated loads applied at all grid points, namely,

$$W_p=\frac{Pw(x_p)}{2}=\frac{1}{2}\sum_{j=1}^{N}Pl_j(\xi_p)w_j=\frac{1}{2}\sum_{j=1}^{N}P_jw_j, \tag{2.14}$$

where W_p is the work done by the concentrated load P, $\xi_p=2x_p/L-1$ and $l_j(\xi)$ is the Lagrange interpolation function defined by

$$l_j(\xi)=\frac{(\xi-\xi_1)(\xi-\xi_2)\cdots(\xi-\xi_{j-1})(\xi-\xi_{j+1})\cdots(\xi-\xi_N)}{(\xi_j-\xi_1)(\xi_j-\xi_2)\cdots(\xi_j-\xi_{j-1})(\xi_j-\xi_{j+1})\cdots(\xi_j-\xi_N)}=\prod_{k=1,\ k\neq j,}^{N}\frac{\xi-\xi_k}{\xi_j-\xi_k}. \tag{2.15}$$

From Eq. (2.14) one has

$$P_j=Pl_j(\xi_p),\quad j=1,2,\cdots,N. \tag{2.16}$$

With the proposed work-equivalent method, Eq. (2.13) is now modified as

$$F_i=2P_i/(LH_i)=2Pl_i(\xi_p)/(LH_i),\quad i=2,3,\cdots,N-1. \tag{2.17}$$

It is easy to show that Eq. (2.17) will be reduced to Eq. (2.13) if ξ_p is one of the integration point, since $l_p(\xi_p)=1$ and $l_j(\xi_p)=0$ $(j\neq p)$.

Since the small region where the load is linearly distributed [15] is twice of the one where the load is uniformly distributed [14], it is easy to show that the methods in [14,15] are equivalent to using the trapezoidal rule for the numerical integration of the governing equation. Therefore, with the increase of the number of grid points accurate results can also be obtained by using the method in [14] or [15] to deal with the point load.

Although the weighting coefficients of the first to fourth order derivatives can be computed explicitly, however, the method of the matrix multiplication is used to build-in one of the two boundary conditions for accuracy considerations. Two methods of modification of weighting coefficients, denoted by MMWC-1 [12, 19] and MMWC-3 [12, 20], are used to implement the simply supported and clamped boundary conditions.

Denote A_{ij}, B_{ij}, D_{ij} the weighting coefficients of the first, second and fourth order derivatives with respect to x. Then A_{ij} can be explicitly computed by [10]

$$A_{ij}=\frac{dl_j(x_i)}{dx}=\begin{cases} \displaystyle\prod_{k=1,\ k\neq i,j,}^{N}(x_i-x_k)\Big/\prod_{k=1,\ k\neq j,}^{N}(x_j-x_k), & i\neq j, \\ \displaystyle\sum_{k=1,\ k\neq i,}^{N}\frac{1}{(x_i-x_k)}, & i=j, \end{cases} \tag{2.18}$$

https://doi.org/10.4208/aamm.2014.m844 Published online by Cambridge University Press

where $l_j(x)$ is Lagrange interpolation functions.

For a beam simply supported at both ends, called the SS beam, MMWC-1 is used. The weighting coefficients B_{ij} and D_{ij} are computed by

$$B_{ij}=\sum_{k=1}^{N}A_{ik}A_{kj},\quad D_{ij}=\sum_{k=2}^{N-1}B_{ik}B_{kj},\quad i,j=1,2,\cdots,N. \tag{2.19}$$

It is seen that MMWC-1 is very simple, only the summation range is slightly changed to build-in the condition of $w^{(2)}=0$ during the computation of D_{ij}.

For a beam clamped at both ends, called the CC beam, MMWC-3 is used. The weighting coefficients B_{ij} and D_{ij} are computed by

$$B_{ij}=\sum_{k=2}^{N-1}A_{ik}A_{kj},\quad i=1,N,\quad j=1,2,\cdots,N, \tag{2.20a}$$

$$B_{ij}=\sum_{k=1}^{N}A_{ik}A_{kj},\quad i=2,3,\cdots,N-1,\quad j=1,2,\cdots,N, \tag{2.20b}$$

$$\overline{B}_{ij}=\sum_{k=1}^{N}A_{ik}A_{kj},\quad i,j=1,2,\cdots,N, \tag{2.20c}$$

$$D_{ij}=\sum_{k=1}^{N}\overline{B}_{ik}B_{kj},\quad i,j=1,2,\cdots,N. \tag{2.20d}$$

Note that the zero first order derivatives at two end points have been built-in during the formulation of B_{ij} at two end points.

For beam clamped at $x=0$ and simply supported at $x=L$, called the CS beam, MMWC-4 [12] is used to build-in the zero first order derivative at $x=0$ and MMWC-1 is used to build-in the zero second order derivative at $x=L$. The weighting coefficients B_{ij} and D_{ij} are computed by

$$B_{1j}=\sum_{k=2}^{N}A_{1k}A_{kj},\qquad j=1,2,\cdots,N, \tag{2.21a}$$

$$B_{ij}=\sum_{k=1}^{N}A_{ik}A_{kj},\qquad i=2,3,\cdots,N,\quad j=1,2,\cdots,N, \tag{2.21b}$$

$$\overline{B}_{ij}=\sum_{k=1}^{N}A_{ik}A_{kj},\qquad i,j=1,2,\cdots,N, \tag{2.21c}$$

$$D_{ij}=\sum_{k=1}^{N-1}\overline{B}_{ik}B_{kj},\qquad i,j=1,2,\cdots,N. \tag{2.21d}$$

Similarly, for beam simply supported at $x=0$ and clamped at $x=L$, called the SC beam,

https://doi.org/10.4208/aamm.2014.m844 Published online by Cambridge University Press

the weighting coefficients B_{ij} and D_{ij} are computed by

$$B_{ij}=\sum_{k=1}^{N}A_{ik}A_{kj}, \qquad i=1,2,\cdots,N-1, \quad j=1,2,\cdots,N, \tag{2.22a}$$

$$B_{Nj}=\sum_{k=1}^{N-1}A_{Nk}A_{kj}, \qquad j=1,2,\cdots,N, \tag{2.22b}$$

$$\overline{B}_{ij}=\sum_{k=1}^{N}A_{ik}A_{kj}, \qquad i,j=1,2,\cdots,N, \tag{2.22c}$$

$$D_{ij}=\sum_{k=2}^{N}\overline{B}_{ik}B_{kj}, \qquad i,j=1,2,\cdots,N. \tag{2.22d}$$

After eliminating the zero deflections at two end points, Eq. (2.12) can be written as following matrix form,

$$[\overline{D}]\{\overline{w}\}=\{\overline{F}\}, \tag{2.23}$$

where the over bar means that the dimension of vectors is not N but $(N-2)$ and the dimension of the matrix is not $N\times N$ but $(N-2)\times(N-2)$ for the four combinations of boundary conditions to be considered.

The non-zero deflection at all inner grid points can be obtained by matrix inversion, namely,

$$\{\overline{w}\}=[\overline{D}]^{-1}\{\overline{F}\}. \tag{2.24}$$

The bending moment at all grid points, denoted by $\overline{M}_i$, can be computed by

$$\overline{M}_i=EI\sum_{k=2}^{N-1}B_{ik}\overline{w}_{(k-1)}, \qquad i=1,2,\cdots,N. \tag{2.25}$$

2.2 Forced vibration of a beam carrying a moving point load

Consider an Euler-Bernoulli beam of length L under a moving point load P at location $x_p(t)=vt$ $(0\le t\le L/v)$. The governing equation is given by

$$\rho A\frac{d^2w(x,t)}{dt^2}+EI\frac{d^4w(x,t)}{dx^4}=P\delta(x-vt) \tag{2.26}$$

or

$$\rho A\ddot{w}+EIw^{(4)}=P\delta(x-vt), \tag{2.27}$$

where ρA is the mass per unit length, v is the velocity of the moving load, and t is the time.

https://doi.org/10.4208/aamm.2014.m844 Published online by Cambridge University Press

Similar procedures to the ones presented in Section 2.1 are followed. The moving point load is firstly work-equivalent to loads applied at all grid points and then Eq. (2.27) is numerically integrated. Thus one has

$$\rho A\ddot{w}_i+EIw_i^{(4)}=F_i,\quad i=2,3,\cdots,N-1, \tag{2.28}$$

where

$$F_i=2P_i/(LH_i)=2Pl_i(vt)/(LH_i),\quad i=2,3,\cdots,N-1. \tag{2.29}$$

In terms of differential quadrature, Eq. (2.28) becomes

$$\rho A\ddot{w}_i+EI\sum_{j=1}^{N}D_{ij}w_j=F_i,\quad i=2,3,\cdots,N-1. \tag{2.30}$$

For the four combinations of boundary conditions, $w_1=w_N=0$ and the other boundary condition has been built-in already. Thus, the following matrix equation is obtained,

$$\left[\overline{M}\right]\left\{\ddot{\overline{w}}\right\}+\left[\overline{D}\right]\left\{\overline{w}\right\}=\left\{\overline{F}(t)\right\}, \tag{2.31}$$

where $[\overline{D}]$ is the weighting coefficient matrix of the fourth order derivative with respect to x, the same as the one in Eq. (2.23), $\{\overline{F}(t)\}$ is defined by Eq. (2.29), and $[\overline{M}]$ is the mass matrix defined by

$$\left[\overline{M}\right]=\rho A\left[\overline{I}\right], \tag{2.32}$$

where $[\overline{I}]$ is a unit matrix. Again the over bar in Eq. (2.31) and Eq. (2.32) means that the dimension of vectors is $(N-2)$ and the dimension of the matrices is $(N-2)\times(N-2)$.

Due to the fact of that the mass matrix is a diagonal matrix, a crucial reduction of the complexity and the cost of the numerical time integration can be achieved. The set of the second-order ordinary differential equations in time, Eq. (2.31), can be efficiently integrated by employing the central finite difference method, namely,

$$\frac{1}{\Delta t^2}[\overline{M}]\{\overline{w}\}_{t+\Delta t}=\{\overline{F}\}_t-\left([\overline{D}]-\frac{2}{\Delta t^2}[\overline{M}]\right)\{\overline{w}\}_t-\frac{1}{\Delta t^2}[\overline{M}]\{\overline{w}\}_{t-\Delta t} \tag{2.33}$$

or

$$\{\overline{w}\}_{t+\Delta t}=\left(\Delta t^2/\rho A\right)\left(\{\overline{F}\}_t-[\overline{D}]\{\overline{w}\}_t\right)+2\{\overline{w}\}_t-\{\overline{w}\}_{t-\Delta t}, \tag{2.34}$$

where Δt is the time step.

Once deflection is known, the bending moment at all grid points, denoted by $(\overline{M}_i)_{t+\Delta t}$ can be computed by

$$(\overline{M}_i)_{t+\Delta t}=EI\sum_{k=2}^{N-1}B_{ik}\left(\overline{w}_{(k-1)}\right)_{t+\Delta t},\quad i=1,2,\cdots,N. \tag{2.35}$$

https://doi.org/10.4208/aamm.2014.m844 Published online by Cambridge University Press

It should be emphasized that the central finite difference method is a conditionally stable method, $\Delta t \leq 2/\omega_n$, where ω_n is the highest natural frequency. Therefore, numerical instability would have occurred if the matrix $[\overline{D}]$ had contained spurious complex eigenvalues. Numerical experience shows that adopting the grid spacing, $\{-1, \eta_i (i = 2,3,\cdots,N-1), +1\}$, where η_i are the $(N-2)$ Gauss integration points, will eliminate the spurious complex eigenvalues for all four combinations of boundary conditions.

3 Results and discussion

For verifications, the modified DQM is used to analyze static and dynamic problems of beams under a stationary or a moving point load. Three examples, not solved successfully by directly using the DQM before, are given and four combinations of boundary conditions are considered.

Example 3.1. Consider first an SS beam subjected to a stationary concentrated load P at point x_p, shown in Fig. 1. The length of the beam is L and the bending rigidity is EI. The loading position x_p takes the values of $0.5L$, $0.6L$, $0.7L$, $0.8L$, $0.9L$ and $0.99L$, respectively.

The percentage error of the central deflection is defined by

$$Er\% = (w_{DQM} - w_{exact})/w_{exact} * 100\%, \tag{3.1}$$

where w_{DQM} and w_{exact} denote the results obtained by the modified DQM and analytical method, respectively.

The analytical solution at middle point $(x = L/2)$ of an SS beam is given by

$$w_{exact} = \frac{P(L-x_p)(8Lx_p - 4x_p^2 - L^2)}{48EI}, \quad (x_p \geq L/2). \tag{3.2}$$

For convergence studies, different numbers of grid points are tried. The percentage errors of the central deflection obtained by the modified DQM are listed in Table 1. It is seen that the solution accuracy is high. With $N = 9$, the percentage error has already been within 1%.

To show the accuracy of the DQ solution at other points, comparisons between the DQ data and exact solutions are made in Fig. 2, where symbol $W*100$ is the deflection coefficient defined by

$$W*100 = \frac{100EIw}{PL^3}. \tag{3.3}$$

Two sets of grid points are shown, one is $N = 7$ and the other $N = 15$. The concentrated load is applied at $0.8L$, which is approximately a grid point when N is 15 but is absolutely not a grid point when N is 7. It is seen that the accuracy of the deflection obtained by the modified DQM at other points is also high.

https://doi.org/10.4208/aamm.2014.m844 Published online by Cambridge University Press

Table 1: Percentage error ($Er\%$) of the deflection at middle point for SS beam under a concentrated load at different locations x_p.

N	7	9	11	13	15	17	19	21
$x_p/L=0.5$	-0.1963	-0.0954	-0.0523	-0.0315	-0.0204	-0.0139	-0.0099	-0.0073
$x_p/L=0.6$	0.0703	0.0579	-0.0383	0.0223	0.0112	0.0044	0.0005	-0.0014
$x_p/L=0.7$	0.1554	0.0123	-0.0221	-0.0186	0.0073	0.0007	0.0035	0.0028
$x_p/L=0.8$	-0.1662	-0.0757	0.0071	0.0191	0.0036	-0.0054	-0.0032	0.0012
$x_p/L=0.9$	-0.1551	0.1286	-0.0085	-0.0244	0.0101	0.0045	-0.0054	0.0002
$x_p/L=0.99$	1.6733	-0.6628	0.2949	-0.1349	0.0587	-0.0212	0.0030	0.0051

The bending moment is an important design variable in engineering practice. Fig. 3 shows the comparisons of the bending moment between DQ data and exact solutions. The symbol M is the bending moment coefficient defined by

$$M=\frac{\overline{M}}{PL}, \tag{3.4}$$

where $\overline{M}$ is the bending moment.

From Fig. 3, it is seen that the accuracy of the bending moment coefficients obtained by the modified DQM at all grid points is also high. Numerical results reveal that the advantage of the ordinary DQM has been retained. It should be pointed out that the accuracy of the bending moment is slightly lower than the one of the deflection. This is slightly different from the ordinary DQM and may be caused by the numerical integration of the differential equation, i.e., Eq. (2.8).

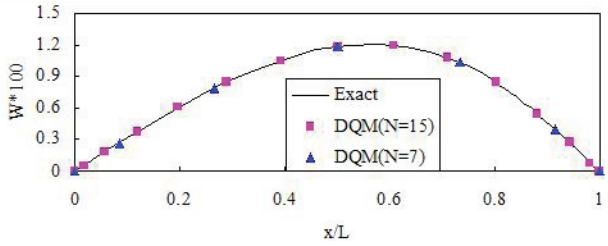


Figure 2: Comparison of exact deflection with DQ solution ($x_p/L=0.8$).

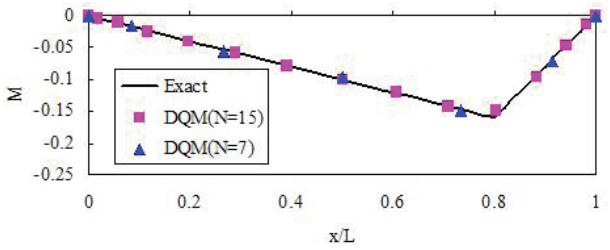


Figure 3: Comparison of exact bending moment with DQ solution ($x_p/L=0.8$).

https://doi.org/10.4208/aamm.2014.m844 Published online by Cambridge University Press

Example 3.2. Consider next an SS beam subjected to a moving point load P at a velocity v. In this case, $x_p = vt$. The length of the beam is L, the bending rigidity is EI, and the mass per unit length is ρA, respectively.

Denote $\tau = L/v$ and $\alpha = T_1/2\tau$, where T_1 is the period of the lowest vibration mode of the beam. For the beam simply supported at both ends, the period of the lowest vibration mode is $T_1 = 2L^2\sqrt{\rho A/EI}/\pi$ [21].

For comparisons, α takes the values of 0.125, 0.25, 0.5 and 0.999. The initial conditions are

$$w(x,0) = \frac{\partial w(x,0)}{\partial t} = 0, \qquad 0 \le x \le L. \tag{3.5}$$

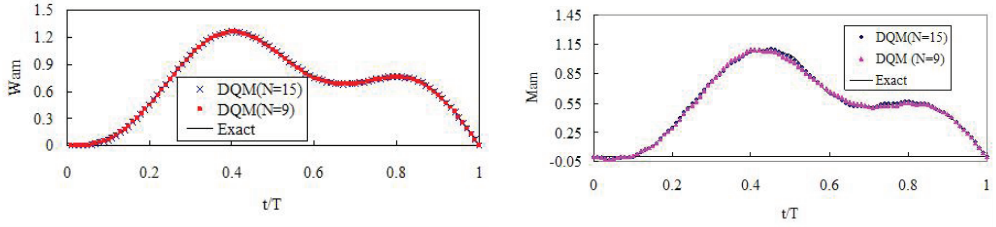
The dynamic magnification factors of deflection and bending moment at the mid-span, denoted by W_{am} and M_{am}, are defined as

$$\begin{cases} W_{am} = w(x = L/2, t)/(PL^3/\beta_w EI), \\ M_{am} = \overline{M}(x = L/2, t)/(-PL/\beta_M), \end{cases} \qquad 0 < t \le \tau, \tag{3.6}$$

where w and $\overline{M}$ are the dynamic deflection and bending moment of the beam, β_w equals to 48 and β_M equals to 4 for the beam simply supported at both ends.

Analytical solutions given by Olsson [22] are used for comparisons. The so called exact solution shown in Figs. 4 and 5 is obtained by using forty series terms taken from [22]. It is observed that the analytical deflection is accurate enough but the analytical bending moment seems not very accurate, since the theoretical curves are not so smooth.

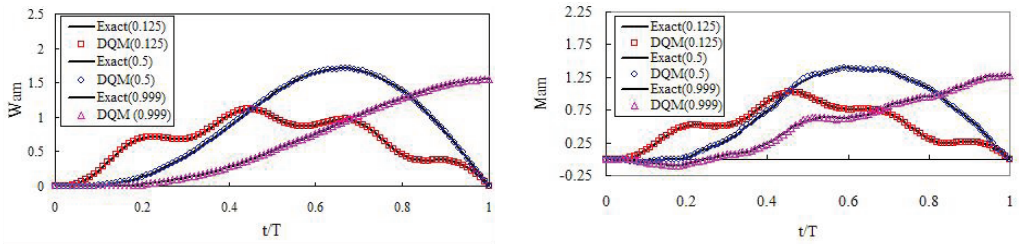
Fig. 4 shows the comparisons of the dynamic magnification factors of deflection and bending moment at the mid-span for the case of $\alpha = 0.25$. Two sets of grid points, $N = 9$ and $N = 15$, are used in the analysis. It is seen that both W_{am} and M_{am} agree well with analytical solutions and the modified DQM with two different numbers of grid points yields similar accurate results. Even with $N = 7$, dynamic magnification factors of deflection is almost the same as the analytical solution shown in Fig. 4. It is observed that, however, the convergence rate of the dynamic magnification factor of bending moment is slightly lower than the convergence rate of the dynamic magnification factor of deflection. Similar phenomenon is observed in the series solutions [22]. Thus $N = 19$ is used in obtaining results shown in Figs. 5-9 for accuracy considerations.



(a) (b)

Figure 4: Comparisons of dynamic magnification factors (a) W_{am} and (b) M_{am} ($\alpha = 0.25$).

https://doi.org/10.4208/aamm.2014.m844 Published online by Cambridge University Press



(a) (b)

Figure 5: Comparisons of dynamic magnification factors (a) W_{am} and (b) M_{am} ($\alpha=0.125,0.5,0.999$).

Fig. 5 shows the comparisons of the dynamic magnification factors of deflection and bending moment at the mid-span for the case of $\alpha=0.125$, 0.5, and 0.999. It is seen that both W_{am} and M_{am} agree well with analytical solutions.

Table 2 shows the comparisons of the maximum dynamic magnification factors W_{am} and M_{am} at the mid-span to analytical solutions and finite element results. It is seen that the maximum W_{am} is the same as the analytical solutions, more accurate than the finite element data. While the accuracy of the maximum M_{am} is slightly lower than the one of the maximum W_{am}. The possible reason may be due to the numerical integration of the differential equation, i.e., Eq. (2.8). For readers' reference, a FORTRAN program is included in appendix which can be used to obtain the results of Example 3.2.

Table 2: Maximum dynamic magnification factors for mid-span displacement W_{am} and mid-span moment M_{am}.

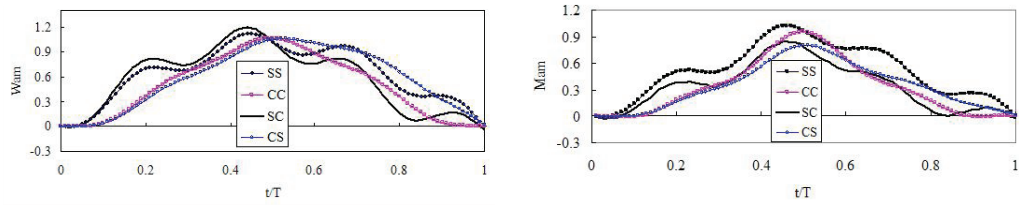
α	W_{am}			M_{am}		
	Exact [22]	Present	FEM [22]	Exact [22]	Present	FEM [22]
0.125	1.121	1.121	1.122	1.027	1.031	1.031
0.25	1.258	1.258	1.259	1.089	1.099	1.082
0.5	1.705	1.705	1.706	1.389	1.389	1.390
1.0	1.548	1.548	1.550	1.273	1.273	1.286

Example 3.3. Consider beams subjected to a moving point load P at a velocity v. Geometry and material parameters are the same as the ones in Example 3.2. Four combinations of boundary conditions, i.e., SS, CC, SC, and CS, are considered. Parameter $\alpha=T_1/2\tau$ takes the values of 0.125 and 0.875. Note that the period of the lowest vibration mode of the CC and CS (or SC) beams are $T_1=0.28084(L^2\sqrt{\rho A/EI})$ and $T_1=0.40752(L^2\sqrt{\rho A/EI})$ [21], different from the one of the SS beam.

The dynamic magnification factors of deflection and bending moment at the mid-span, W_{am} and M_{am}, are also defined by Eq. (3.6). β_w equals to 192 and 768/7 for the CC and CS (or SC) beams, and β_M equals to 8 and 16/3 for the CC and CS (or SC) beams, respectively.

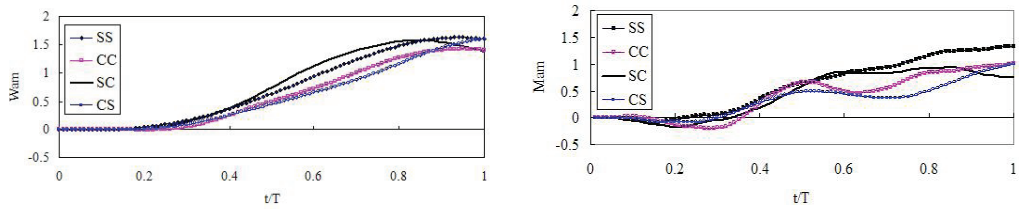
Figs. 6 and 7 show the dynamic magnification factors of deflection and bending moment at the mid-span for the cases of $\alpha=0.125$ and 0.875. It is seen that boundary con-

https://doi.org/10.4208/aamm.2014.m844 Published online by Cambridge University Press



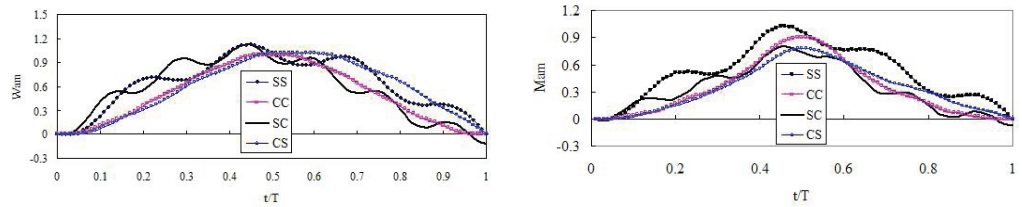
(a) (b)

Figure 6: Influences of boundary conditions on the dynamic magnification factors (a) W_{am} and (b) M_{am} ($\alpha=0.125$).



(a) (b)

Figure 7: Influences of boundary conditions on the dynamic magnification factors (a) W_{am} and (b) M_{am} ($\alpha=0.875$).



(a) (b)

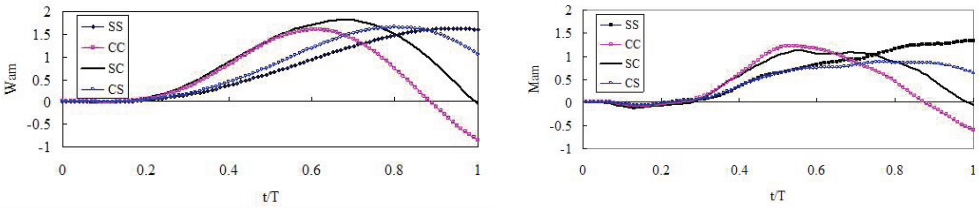
Figure 8: Influences of boundary conditions on the dynamic magnification factors (a) W_{am} and (b) M_{am} ($\bar{\alpha}=0.125$).

ditions have appreciate effect on the deflection and bending moment. The W_{am} curves of the CC and CS beams are smoother than the other two when $\alpha=0.125$. On the opposite, the M_{am} curves of the SS and SC beams are smoother than the other two when $\alpha=0.875$. Note that for the same α the velocity is different, since $\alpha=vT_1/2L$ and T_1 is different for different combinations of boundary conditions.

If the velocity is the same, e.g., $\bar{\alpha}=\overline{T}_1/2\tau$, where $\overline{T}_1=2L^2\sqrt{\rho A/EI}/\pi$ for all combinations of boundary conditions, the dynamic magnification factors of deflection and bending moment at the mid-span for the cases of $\bar{\alpha}=0.125$ and 0.875 are shown in Figs. 8 and 9. Comparisons of the two figures with Figs. 6 and 7 reveal that differences do exist. The difference between Figs. 7 and 9 is larger than the difference between Figs. 6 and 8.

It is reported that the boundary conditions affect the rate of convergence. Stiffer

https://doi.org/10.4208/aamm.2014.m844 Published online by Cambridge University Press



(a) (b)

Figure 9: Influences of boundary conditions on the dynamic magnification factors (a) W_{am} and (b) M_{am} ($\bar{\alpha}=0.875$).

boundary conditions (i.e., clamped-clamped) require a larger number of grid points during static analysis by using the DQM [15], a great number of elements for analyzing moving load problem by using FEM [18, 23], or more terms for analyzing moving load problem by using the Ritz method [17]. Besides the greater the traveling velocity to the fundamental frequency of the beam, the finer mesh is required to minimum the error [23]. Therefore, a convergence study is performed by using the modified DQM with different numbers of grid points. To investigate the effect of boundary conditions on the rate of convergence, beams with simply supported-simply supported and clamped-clamped boundary conditions are considered. Results are listed in Tables 3 and 4. For comparisons, the available analytical or numerical data are also included.

It is seen that the rate of convergence for the present method is slightly lower as compared to the static case but also high. The modified DQM with $N=17$ can yield accurate results for both cases considered. The boundary conditions have little effect on the rate of convergence. For the C-C beam, the DQ result for higher traveling velocity is slightly lower than the available finite element datum. It is believed that present results should be more accurate than the finite element data, since the results remain unchanged

Table 3: Maximum dynamic magnification factors for mid-span displacement W_{am} of beams with both ends simply supported.

α	$N=11$	$N=13$	$N=15$	$N=17$	$N=19$	$N=21$	Analytical [23]	FEM [23]
0.25	1.2581	1.2579	1.2578	1.2577	1.2576	1.2576	1.2577	1.258
0.5	1.7055	1.7054	1.7054	1.7054	1.7054	1.7054	1.7053	1.707
0.617	1.7316	1.7316	1.7316	1.7317	1.7317	1.7317	1.7316	1.732
0.75	1.7019	1.7016	1.7015	1.7016	1.7016	1.7016	1.7016	1.702

Table 4: Maximum dynamic magnification factors for mid-span displacement W_{am} of beams with both ends clamped.

α	$N=11$	$N=13$	$N=15$	$N=17$	$N=19$	$N=21$	FEM [23]
0.25	1.303	1.310	1.308	1.309	1.310	1.310	1.311
0.5	1.640	1.637	1.636	1.638	1.638	1.638	1.638
0.75	1.530	1.534	1.532	1.533	1.532	1.532	1.551

https://doi.org/10.4208/aamm.2014.m844 Published online by Cambridge University Press

by using the DQM with $N=31$. The possible reason is that insufficient number of beam elements is used in [23] since the traveling velocity to the fundamental frequency of the beam is greater than the other two presented in Table 4.

4 Conclusions

In this paper, a modified DQM is proposed to solve the partial differential equations involving time dependent Dirac-delta functions. Two important modifications are made. One is that the stationary or moving point load is work-equivalent to loads applied at all grid points; the other is that the governing equation is numerically integrated before it is discretized in terms of differential quadrature. The capability and reliability of the proposed method are demonstrated through the solution of Euler-Bernoulli beams under a stationary or a moving point load. Comparisons to analytical solutions and existing finite element data verify that the proposed method is reliable and accurate. The boundary conditions have little effect on the rate of convergence. It is demonstrated that the compactness and computational efficiency of the DQM are retained in solving the partial differential equations with time dependent Dirac-delta functions. The present research extends the application range of the differential quadrature method.

Appendix

The FORTRAN codes for solving the problem in Example 3.2 are listed below for readers' reference. Note that the two missing subroutines, i.e., subroutines named GRULE and DQSS, can be found in [12] on pages 250–254. The subroutine GRULE computes the N integration points (stored in XI) and corresponding weights (stored in WII) used in Gaussian quadrature. The subroutine DQSS computes the weighting coefficients of the first to fourth order derivatives with respect to x for both ends simply supported and stored in AX, BX, CX and DX, respectively. The zero second order derivatives at two end points have been considered in obtaining CX and DX. Since only non-dimensional quantities are needed, thus the bending rigidity EI and the mass per unit length ρA of the beam are not included in the program and the beam length is set to 1. In this case the fundamental circular frequency of an S-S beam is π^2.

```
IMPLICIT REAL*8 (A-H,O-Z)
PARAMETER (N=19, NX=N,NN=NX-2) ! S-S beam, N-odd number only
CHARACTER FILE_OUT*50
DIMENSION AX(NX,NX),BX(NX,NX) ), CX(NX,NX), DX(NX,NX), XX(NX)
DIMENSION GG(NN,NN),X(NX),WI(NX),H(N),BBX(NN,NN)
DIMENSION UI0(NN),UI1(NN),UI2(NN),F0(NN),F1(NN)
DIMENSION WII(NN),XI(NN),Y(N)
```

https://doi.org/10.4208/aamm.2014.m844 Published online by Cambridge University Press

```
C  Input filename of output
      WRITE (*,' (a)')' Enter output file name (< 50 characters )'
      READ (*,' (a)') FILE_OUT
      OPEN (UNIT=6, STATUS='UNKNOWN',FILE=FILE_OUT)
      PI=DATAN (1.0D0)*4.0D0
      A=1.0D0 ! Length of the beam and is assumed as unity
      ALPHA=0.25D0 ! The smaller the alpha, the larger number of integration steps is
      needed.
      V=PI*ALPHA ! Fundamental circular frequency is PI*PI. Please refer to the notes
      above
      TAU=1.0D0/V
      NC=(NN+1)/2 ! Middle point (N-odd number only)
      CALL GRULE (N-2,XI,WII,Y)
      XX(1)=0.0D0
      XX(N)=A
      X(1)= -1.0D0
      X(N)= 1.0D0
      DO I=1,N-2
         X (I+1)=XI(I) ! X[-1,1]
         WI(I+1)=WII(I)
         XX(I+1)=A*(1.0D0+XI(I))/2.0D0 ! XX[0,A]
      ENDDO
      CALL DQSS (NX,XX,AX,BX, CX, DX,Y) ! AX and CX are not used
      DO I=1,NN
      DO J=1,NN
         GG (I,J)=DX(I+1,J+1)
         BBX(I,J)=BX(I+1,J+1)
      ENDDO
      ENDDO
C  Step by step numerical integration by using the central finite difference method
      DO I=1,NN
         UI2(I)=0.0D0
         UI1(I)=0.0D0
```

https://doi.org/10.4208/aamm.2014.m844 Published online by Cambridge University Press

```
ENDDO
WMAX=0.0D0 ! Wam
BMAX=0.0D0 ! Mam
DT=TAU/100000.0D0 ! time step
DT2=DT*DT
T=0.0D0 ! time
DO I=1,100000

    DO J=1,NN
        UI0(J)=UI1(J)
        UI1(J)=UI2(J)
    ENDDO
    T=T+DT
    XP=V*T
    XPP=(XP-A/2)/A*2
    CALL LARG (N,XPP,X,H)
    DO IK=1,NN
        F0(IK)=2.0D0*H(IK+1)/WI(IK+1) ! Eqivalent load
    ENDDO
    CALL SUPERPOSITION (NN,GG,UI1,F1,F0)
    DO J=1,NN
        UI2(J)=DT2*F1(J)+2.0D0*UI1(J)-UI0(J) ! Eq. (2.34)
    ENDDO
    BM=0.0D0
    DO IK=1,NN
        BM=BM-BBX(NC,IK)*UI2(IK)
    ENDDO
    IF (WMAX. LT. UI2(NC)) WMAX=UI2(NC)
    IF (BMAX. LT. BM) BMAX=BM
    IF ((I/1000)*1000.EQ. I) WRITE (6,*) T/TAU,UI2(NC)*48.0D0,BM*4.0D0 ! for
    plots

ENDDO
WRITE (*,*) ALPHA,WMAX*48.0D0,BMAX*4.0D0 ! Output results on screen ! data
in tables.
STOP
END

SUBROUTINE SUPERPOSITION (N,STIFF,UI1,F1,F0)
IMPLICIT REAL*8 (A-H,O-Z)
DIMENSION UI1(N),F1(N),F0(N)
DIMENSION STIFF(N,N)

C  Calculate Fn−[K]{Un}
```

https://doi.org/10.4208/aamm.2014.m844 Published online by Cambridge University Press

```
      DO I=1,N
         F1(I)=F0(I)
      ENDDO
      DO I=1,N
      DO J=1,N
         F1(I)=F1(I)-STIFF(I,J)*UI1(J)
      ENDDO
      ENDDO
      RETURN
      END

SUBROUTINE LARG (N,X,GX,H)
IMPLICIT REAL*8 (A-H,O-Z)
DIMENSION H(N),GX(N)

      DO I=1,N
         H(I)=1.0D0
      DO 3 J=1,N
      IF (I. EQ.J) GOTO 3
      H(I)=H(I)*(X-GX(J))/(GX(I)-GX(J))
      3 CONTINUE
      ENDDO
      RETURN
      END
```

Acknowledgements

The project is partially supported by the Research Fund of State Key Laboratory of Mechanics and Control of Mechanical Structures (Nanjing University of Aeronautics and Astronautics) (Grant No. 0214G02) and the Priority Academic Program Development of Jiangsu Higher Education Institutions.

https://doi.org/10.4208/aamm.2014.m844 Published online by Cambridge University Press

References

[1] R. BELLMAN AND J. CASTI, *Differential quadrature and long term integration*, J. Math. Anal. Appl., 34(2) (1971), pp. 235–238.

[2] R. BELLMAN, B. G. KASHEF AND J. CASTI, *Differential quadrature: a technique for the rapid solution of nonlinear partial differential equations*, J. Comput. Phys., 10 (1972), pp. 40–52.

[3] C. W. BERT, S. K. JANG AND A. G. STRIZ, *Two new approximate methods for analyzing free vibration of structural components,* AIAA J., 26 (1988), pp. 612–618.

[4] T. C. FUNG, *Solving initial value problems by differential quadrature method: Part 1: first order equations*, Int. J. Numer. Methods Eng., 50(6) (2001), pp. 1411–1427.

[5] T. C. FUNG, *Solving initial value problems by differential quadrature method: Part 2: second and higher order equations*, Int. J. Numer. Methods Eng., 50(6) (2001), pp. 1429–1454.

[6] C. SHU, Q. YAO AND K. S. YEO, *Block-marching in time with DQ discretization: an efficient method for time-dependent problems*, Comput. Methods Appl. Mech. Eng., 191 (2001), pp. 4587–4597.

[7] W. CHEN AND M. TANAKA, *A study on time schemes for DRBEM analysis of elastic impact wave*, Comput. Mech., 28 (2002), pp. 331–338.

[8] W. CHEN, C. SHU, W. HE AND T. ZHONG, *The application of special matrix product to differential quadrature solution of geometrically nonlinear bending of orthotropic rectangular plates,* Comput. Struct., 74(1) (2000), pp. 65–76.

[9] C. W. BERT AND M. MALIK, *Differential quadrature method in computational mechanics: A review,* Appl. Mech. Rev., 49 (1996), pp. 1–28.

[10] C. SHU, Differential Quadrature and Its Application in Engineering, London, Springer-Verlag, 2000.

[11] Z. ZONG AND Y. ZHANG, Advanced Differential Quadrature Methods, CRC Press, 2009.

[12] X. WANG, Differential Quadrature and Differential Quadrature Based Element Methods: Theory and Applications, Elsevier Inc., 2015.

[13] B. ENGQUIST, A. K. TORNBERG AND R. TSAI, *Discretization of Dirac delta functions in level set methods,* J. Comput. Phys., 207 (2005), pp. 28–51.

[14] C. ZHANG, Z. HU AND Z. ZHONG, *Wavelet-based differential quadrature method for the analysis of graded composite beam under concentrated loading,* Acta. Mechnica Solida Sinica, 27 (2006), pp. 38–42.

[15] H. T. HAN, Z. ZHANG AND Z. X. LU, *Differential quadrature (DQ) method of discontinous problem*, J. Mech. Strength, 32(2) (2010), pp. 333–337.

[16] X. WANG AND H. GU, *Static analysis of frame structures by the differential quadrature element method,* Int. J. Numer. Methods Eng., 40 (1997), pp. 759–772.

[17] S. M. R. KHALILI, A. A. JAFARI AND S. A. EFTEKHARI, *A mixed Ritz-DQ method for forced vibration of functionally graded beams carrying moving loads,* Compos. Struct., 92(10) (2010), pp. 2497–2511.

[18] A. A. JAFARI AND S. A. EFTEKHARI, *A new mixed finite element-differential quadrature formulation for forced vibration of beams carrying moving loads,* ASME J. Appl. Mech., 2011, 78(1) (2011), pp. 011–020.

[19] X. WANG AND C. W. BERT, *A new approach in applying of differential quadrature to static and free vibrational analyses of beams and plates*, J. Sound Vib., 162(3) (1993), pp. 566–572.

[20] X. WANG, F. LIU, X. WANG AND L. GAN, *New approaches in application of differential quadrature method for fourth-order differential equations,* Commun. Numer. Methods Eng., 21(2) (2005), pp. 61–71.

https://doi.org/10.4208/aamm.2014.m844 Published online by Cambridge University Press

[21] A. W. LEISSA, *The free vibration of rectangular plates,* J. Sound Vib., 31(3) (1973), pp. 257–293.
[22] M. OLSSON, *On the fundamental moving load problem,* J. Sound Vib., 145(2) (1991), pp. 299–307.
[23] J. R. RIEKER, Y. H. LIN AND M. W. TRETHEWEY, *Discretization considerations in moving load finite element beam models,* Finite Elem. Anal. Des., 21 (1996), pp. 129–144.

https://doi.org/10.4208/aamm.2014.m844 Published online by Cambridge University Press